Table 1. Physical properties of PP nanocomposites.

M_w	M_w/M_n	T_m [°C]	Isotacticity [triad %]	Clay loading [wt.-%]
181 000	2.16	158	98.5	10.5

0.1 wt.-%, the Young's modulus of the PP is in the range of 220 to 260 kpsi, which is comparable to PP made by the solution process. This significant (over 2×) improvement in Young's modulus may help these in-situ PP nanocomposites to compete with costly engineering plastics. Other improved properties of the PP–clay nanocomposites made in this work are a reduced thermal expansion coefficient, improved melt flow strength, increased heat-distortion temperatures, and lowered gas diffusion coefficient.

In summary, we report on a novel in-situ polymerization approach for manufacturing polyolefin–clay nanocomposites with amazingly improved catalyst efficiency and product performance. These polyolefin nanocomposites have the potential to expand the range of applicability of polyolefins and to compete with engineering thermoplastics.

[1] A. Usuki, Y. Kojima, M. Kawasumi, A. Okada, Y. Fukushima, T. Jurauchi, O. Kamigaito, *J. Mater. Res.* **1993**, *8*, 1179.
[2] Y. Kojima, A. Isilo, M. Kawasumi, A. Okada, Y. Fukushima, T. Kuarauchi, O. Kamigaito, *J. Mater. Res.* **1993**, *8*, 1185.
[3] A. Usuki, M. Kato, A. Okada, T. Kurauchi, *J. Appl. Polym. Sci.* **1997**, *63*, 137.
[4] J. Tudor, L. Willingto, D. O'Hare, *Chem. Commun.* **1997**, 2031.
[5] J. Bergman, H. Chen, E. P. Giannelis, M. G. Thomas, G. W. Coates, *Chem. Commun.* **1999**, 2179.
[6] L. C. Johnson, M. K. Killian, M. Brookhart, *J. Am. Chem. Soc.* **1996**, *118*, 267.
[7] J. Heinemann, P. Reichert, R. Thomann, R. Mulhaupt, *Macromol. Rapid Commun.* **1999**, *20*, 423.
[8] M. Alexandre, P. Dubois, T. Sun, J. M. Garcés, R. Jerome, unpublished.

Chemical Defect Decoration of Carbon Nanotubes**

By *Yuwei Fan,* Marko Burghard,** and *Klaus Kern*

Carbon nanotubes (CNTs), due to their high mechanical strength and outstanding electrical properties, have attracted considerable interest for applications such as field emission,[1,2] mechanically reinforced composite materials,[3] scanning probe microscopy tips,[4] as well as molecular-scale electronic devices such as field-effect transistors[5] or sensors.[6] For most of these potential applications, defects in the CNTs

Fig. 2. a,b) Optical images of clay–PP nanocomposite. c–e) TEM images of the same sample at different magnifications.

on the specific organoclay precursor and the catalyst preparation methods. The crystallinity of the PP polymer in these nanocomposites is around 65 %. The physical properties of a typical PP–clay nanocomposites from this work are summarized in Table 1.

When the powdery PP–clay nanocomposite is compression-molded and tested for mechanical performance, it shows a drastically improved Young's tensile modulus, up to 600 kpsi, which is well above the modulus of highly crystalline PP. Running the same polymerization process with clay loading below

[*] Dr. Y. Fan, Dr. M. Burghard, Prof. K. Kern
Max-Planck-Institut für Festkörperforschung
Heisenbergstrasse 1, D-70569 Stuttgart (Germany)
E-mail: Y.Fan@fkf.mpg.de, M.Burghard@fkf.mpg.de

play a crucial role in performance, reliability, and stability. Moreover, defects are considered as reactive sites during chemical tube modification.[7] The defects in CNTs can be classified into several categories including topological defects (corresponding to the presence of rings other than hexagons, for example pentagon/heptagon pairs), incomplete bonding defects (e.g., vacancies, dislocations, etc.), and chemical defects consisting of atoms/groups covalently attached to the carbon lattice of the tubes. The effect of different types of defects on the electronic structure of CNTs has been investigated theoretically with emphasis on predicting signatures in scanning tunneling microscopy (STM) and spectroscopy (STS).[8,9] On the experimental side, electrical studies on individual single-walled carbon nanotubes (SWCNTs) have revealed the importance of defects in understanding their transport properties.[10,11] The intentional introduction of defects to ropes of SWCNTs by controlled sputtering was reported to lead to strong carrier scattering in the current carrying tubes.[12] Up to now, however, little is known about the density, distribution, and nature of defects in CNTs. This situation is mainly due to the lack of fast and reliable methods to locate defect sites within the tubes. Although STM has been employed to determine the chiral angle of individual SWCNTs,[13,14] as well as to investigate SWCNT intramolecular junctions,[15] it has not been successfully used to locate defects in nanotubes. Electronic spin resonance (ESR) experiments have been performed on SWCNTs,[16] but generally provide only an average measure of the defect density in bulk samples.

Here we report a simple technique for the titration of chemical defects in SWCNTs. The method is based on the formation of Se nanoparticles on the tubes upon exposure to hydrogen selenide (H_2Se) under ambient conditions. A comparative study of highly oriented pyrolytic graphite (HOPG) surfaces, oxidized by O_2 plasma, strongly supports the conclusion that the Se particles grow by site-selective oxidation of H_2Se at surface functionalities containing oxygen atoms.

Treatment with H_2Se was performed on SWCNTs deposited on a Si wafer with a thermally grown SiO_2 layer of 100 nm thickness. Under ambient conditions H_2Se is a gas that is readily oxidized to elemental selenium, as reflected in the standard reduction potential for H_2Se/Se of –0.115 V in acidic aqueous solution.[17] Figure 1A displays an atomic force microscopy (AFM) image of SWCNTs, present as individual tubes and thin tube bundles (3–4 nm in height), before exposure to a H_2Se atmosphere. It is apparent from Figure 1B, which shows the same tubes as in Figure 1A after H_2Se exposure for 2 min, that small Se particles have formed on the tube/bundle surface. These particles are ~8 nm in height, as deduced from the AFM section profile, and are non-equally spaced along the tubes/thin bundles. Selenium nanoparticle formation occurs selectively at the tubes, with almost no particles detectable in the SiO_2 background. Closer inspection of smaller scan size AFM images reveals that the Se particles make intimate contact to the tube surface (see inset of Fig. 1B), with their position varying from on-side to fully on
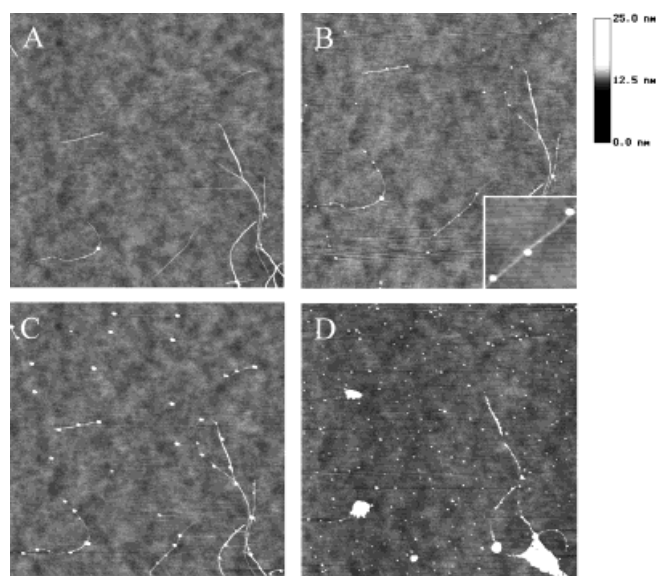

Fig. 1. AFM images (6 × 6 μm^2) displaying the decoration of SWCNTs, deposited on a Si/SiO$_2$ wafer, with Se nanoparticles. A) The tubes before exposure to H$_2$Se. B) Selenium nanoparticles are observed on the same tubes after treatment with H$_2$Se for 2 min; the inset of (B) shows a magnified view of a tube decorated by three Se particles. C) Prolonged H$_2$Se exposure, for 20 min in total, resulted in particles of increased size, but the formation of additional particles is not observed. D) An increased density of Se particles is found after oxygen plasma treatment (30 s) of the same substrate, followed by H$_2$Se exposure for 2 min. Plasma treatment under these conditions almost completely removed the thinner tubes on the left side of the image, whereas the thicker bundle to the right is still present.

top of the tubes. After H_2Se exposure of the same tubes for 20 min in total, the size of the particles increased to ~18 nm, but no additional particles were formed (Fig. 1C). The evaluation of a large number of tubes treated with H_2Se revealed center-to-center particle separations in the range between 200 nm and 600 nm, with an average spacing of ~350 nm. The same sample was then used in additional experiments to test the influence of tube oxidation by O_2 plasma treatment. After a 30 s O_2 plasma treatment and a 2 min exposure to a H_2Se atmosphere, the tubes showed a significantly increased density of Se particles (Fig. 1D). For tubes oxidized under these conditions, the average separation of Se particles was found to be ~200 nm.

To elucidate the mechanism of Se particle formation, we studied the behavior of pristine and modified HOPG surfaces. It is an important result that H_2Se exposure of unmodified HOPG, used as a control sample, yielded an extremely low density of Se particles (~2 per 100 μm^2) located at edge plane sites. Figure 2A displays the AFM image of a freshly cleaved HOPG substrate exposed for 2 min to H_2Se. After O_2 plasma treatment, performed to intentionally introduce defects, and subsequent exposure to H_2Se, a significantly increased number of selenium particles is found in a non-uniform spatial distribution. This is illustrated by the AFM image in Figure 2B showing the same area on the HOPG surface after 10 s in O_2 plasma, and H_2Se exposure for 2 min. The Se particles are preferably deposited at the step edges of the HOPG surface, with a smaller density found within the basal plane regions.
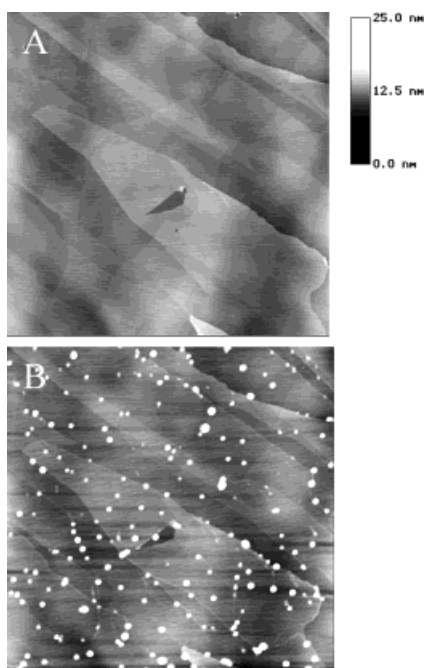
Fig. 2. AFM image (6×6 μm^2) of a freshly cleaved, unmodified HOPG surface exposed to H_2Se for 2 min (A), and the same area after 10 s treatment with oxygen plasma, followed by 2 min exposure to a H_2Se atmosphere (B).

Fig. 3. Consecutive AFM images (2×2 μm^2) of the same area on a HOPG surface, treated for 10 s in oxygen plasma, for the substrate exposed for 10 s to a H_2Se atmosphere (A), the substrate treated in H_2Se atmosphere for 40 s (B), and after H_2Se exposure for 100 s in total (C).

The dependence of the amount of Se nanoparticles obtained as a function of H_2Se exposure time is shown in the AFM images of Figure 3. The HOPG surface modified by 10 s of O_2 plasma treatment, followed by 10 s in H_2Se atmosphere, is depicted in Figure 3A. After this short H_2Se exposure, the Se particles formed are still too small to be clearly visible. It should be noted that the branched structures of tube-like appearance are attributed to folds of graphitic sheets, which are characteristic of cleaved HOPG surfaces, as documented in scanning probe microscopy studies.[18] The same region after a total of 40 s in H_2Se atmosphere is shown in Figure 3B, revealing particles with an average size of 6 nm. Identical to the case of CNTs, additional exposure to H_2Se (+1 min) resulted in Se particles of increased size (~14 nm), while the number of particles remained constant (Fig. 3C).

The fact that almost no Se particles are observed on the unmodified HOPG surface provides evidence that they grow via reaction at specific surface sites, as opposed to a physical deposition of Se particles that may be formed in the gas phase due to oxidation by air. The distribution of the Se particles in Figure 2 is similar to that of evaporated metal particles on HOPG surfaces with intentionally introduced surface defects.[19] It is well documented that HOPG surfaces treated by thermal[20] or electrochemical oxidation[21] possess polar surface groups within pit holes. The presence of such groups was proven, for example, by Raman spectroscopic investigation of thermally pitted HOPG surfaces.[22] Evidently, these groups on the oxidized HOPG surface are able to induce the local oxidation of H_2Se to selenium. Once the formation of selenium starts, the size of the Se particles increases upon further H_2Se exposure, which is explained by an autocatalytic
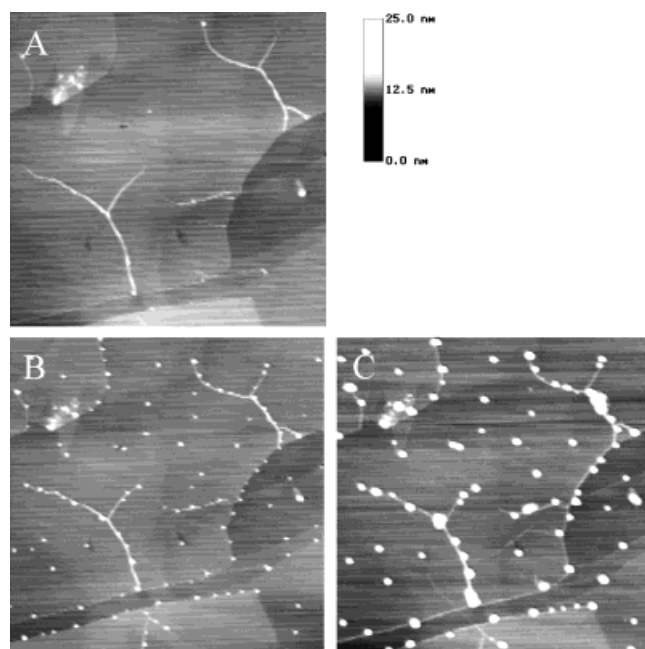
growth mechanism. Similar effects occur in the deposition of antimony on glass surfaces via autocatalytic decomposition of SbH_3 at room temperature. The very small number of Se particles formed on the pristine HOPG is in accordance with the fact that oxide moieties exist only in small density at edge plane sites.[23]

In light of the results obtained for the pristine/oxidized HOPG surface, combined with the expectation that the tubes, due to their curvature, should exhibit a higher reactivity against oxygen than graphite planes, we conclude that oxygen-containing groups are present on the tubes, and play a crucial role in the Se nanoparticle formation. There are two possible types of such groups on SWCNT surfaces that may mediate the site-selective growth of Se particles. First, appropriate functionalities such as quinone structural motives could lead to locally restricted oxidation of H_2Se to selenium. This case would require that such strongly oxidized groups, capable of acting as oxidizers by themselves, exist within the deposited SWCNTs. As an alternative, polar surface functions, for example oxygen ad-atoms or hydroxyl groups, might act as atomic-scale catalysts that promote the oxidation of H_2Se to elemental selenium by the oxygen in air. In order to test the first assumption, we investigated the properties of SWCNTs that were first treated on the substrate with a reducing agent before H_2Se exposure. Since for all of these samples the same average density of Se particles was observed on the CNTs, we exclude the first mechanism. On the contrary, the surface catalytic mechanism gains support from the properties of differently modified SiO_2 surfaces. Whereas only a small number of selenium particles (~25/100 μm^2) is formed on a SiO_2 substrate rendered hydrophobic by attachment of $-Si(CH_3)_3$ sur-

face groups, a high Se particle density (~1.5×10^4/100 μm^2) is observed on SiO$_2$ modified by amino-silanization. The latter result reveals that –Si(OC$_2$H$_5$)$_2$–(CH$_2$)$_3$–NH–(CH$_2$)$_2$–NH$_2$ surface functions, which have polar but no oxidizing character, apparently are able to catalyze the oxidation of H$_2$Se, similar to the above postulated mechanism involving polar groups on the CNTs. It is worth noting that the proposed mechanism bears some resemblance with the decoration of multi-walled carbon nanotubes with metals and metal compounds, reported by Ebbesen et al.[24] In this case, nucleation occurred at oxidized surface groups introduced by gas or liquid phase oxidation.

One possible origin of the polar groups in the SWCNTs is the ultrasonic treatment of the tubes required to disperse them in surfactant solution before deposition on the Si/SiO$_2$ substrate. We investigated the effect of longer sonication times and/or intensities, increased up to 20 s and 150 W/cm^2, respectively. However, we did not find any increase of the average density of deposited Se particles. It is therefore concluded that the relevant functional groups already exist in the pristine SWCNT material, possibly originating from oxidation of atomic-scale defects, created during CNT growth,[25] upon air exposure. The distance between the Se particles on the SWCNTs, which is interpreted to reflect the chemical defect density in the tubes, should represent the maximum distance over which ballistic electrical transport is possible. Noteworthy, Se particle distances between 200 nm and 600 nm, found in our experiments, are in good agreement with the experimentally observed values of the phase coherence length, which fall in the range of 150 nm–750 nm.[26–28]

In summary, we present a straightforward method to identify the location of chemical defects in SWCNTs. The formation of Se nanoparticles via site-selective oxidation of H$_2$Se works under soft conditions at room temperature, and is able to reveal the defects even in individual tubes. In combination with scanning probe or electron microscopy the method can be developed into a rapid screening tool to reveal the defect location in single nanotubes, as well as to determine the average density of chemical defects in carbon nanotube samples. These are important issues for many applications exploiting the tube's electrical and mechanical properties, for which it is imperative to understand the electronic and structural properties not only of the tubes themselves but also of their defects.

Experimental

SWCNT raw material was dispersed in a 1 wt.-% aqueous solution of lithium dodecylsulfate with the aid of ultrasonic agitation (Dr. Hielscher UP 200s, ~40 W/cm^2 applied to a volume of 1 mL for approximately 10 s), and was purified by centrifugation. The tubes were deposited by covering the Si/SiO$_2$ substrate with the purified suspension for 30 min, followed by rinsing with pure water and drying under a stream of argon. Treatment with H$_2$Se was accomplished by placing the substrate in a closed glass vessel (~60 cm^3 volume) in which ~10 mg of aluminum selenide was reacted with ~50 μL of water. In this way, the tubes on the substrate were exposed to a concentration of approximately 2×10^3 mol/m^3 of H$_2$Se at ambient temperature. In our experiments, we mainly used SWCNT material produced by the arc discharge method, and kindly supplied by Prof. P. Bernier (University of Montpellier, France). Investi-

gation of commercial SWCNT material prepared by arc discharge (CARBO-LEX, Lexington, USA), or laser ablation SWCNTs (Rice University, Houston, USA) showed the same average selenium particle distance within ±20 nm. The SWCNTs were investigated by atomic force microscopy (Digital Instruments Nanoscope IIIa) using standard silicon cantilevers in tapping mode. Two perpendicular scratches were used as position markers in order to repeatedly find the same tubes on the substrate. In the pre-reduction experiments, the SWCNTs were reduced immediately before H$_2$Se exposure by one of the following reducing agents: potassium borohydride, sodium dithionite, hydrazine, or thioglycerol. These treatments were performed in aqueous medium at room temperature and various pH values in the range between 1 and 12, in order to cover a broad range of reducing conditions. The HOPG (ZYA grade) was purchased from NT-MDT in Moscow, Russia. All oxygen plasma treatments were performed at 200 W and a pressure of 1.33 mbar.

[1] S. Fan, M. G. Chapline, N. R. Franklin, T. W. Tombler, A. M. Cassel, H. Dai, *Science* **1999**, *283*, 512.
[2] W. A. de Heer, A. Châtelain, D. Ugarte, *Science* **1995**, *270*, 1179.
[3] L. S. Schadler, S. C. Giannaris, P. M. Ajayan, *Appl. Phys. Lett.* **1998**, *73*, 3842.
[4] S. S. Wong, E. Joselevich, A. T. Woolley, C. L. Cheung, C. M. Lieber, *Nature* **1998**, *394*, 52.
[5] S. J. Tans, A. R. M. Verschueren, C. Dekker, *Nature* **1998**, *393*, 49.
[6] J. Kong, N. R. Franklin, C. Zhou, M. G. Chapline, S. Peng, K. Cho, H. Dai, *Science* **2000**, *287*, 622.
[7] J. L. Bahr, J. Yang, D. V. Kosynkin, M. J. Bronikowski, R. E. Smalley, J. M. Tour, *J. Am. Chem. Soc.* **2001**, *123*, 6536.
[8] D. Orlikowski, M. Buongiorno Nardelli, J. Bernholc, C. Roland, *Phys. Rev. B* **2000**, *61*, 14 194.
[9] F. Wei, J.-Z. Zhu, H.-M. Chen, *J. Phys.: Condens. Matter* **2000**, *12*, 8617.
[10] M. Bockrath, W. Liang, D. Bozovic, J. H. Hafner, C. M. Lieber, M. Tinkham, H. Park, *Science* **2001**, *291*, 283.
[11] D. Bozovic, M. Bockrath, J. H. Hafner, C. M. Lieber, H. Park, M. Tinkham, *Appl. Phys. Lett.* **2001**, *78*, 3693.
[12] H. Stahl, J. Appenzeller, R. Martel, P. Avouris, B. Lengeler, *Phys. Rev. Lett.* **2000**, *85*, 5186.
[13] J. W. G. Wildoer, L. C. Venema, A. G. Rinzler, R. E. Smalley, C. Dekker, *Nature* **1998**, *391*, 59.
[14] J. W. Odom, J.-L. Huang, P. Kim, C. M. Lieber, *Nature* **1998**, *391*, 62.
[15] M. Ouyang, J.-L. Huang, C. L. Cheung, C. M. Lieber, *Science* **2001**, *291*, 97.
[16] M. Kosaka, T. W. Ebbesen, H. Hinra, K. Tanigaki, *Chem. Phys. Lett.* **1994**, *225*, 161.
[17] F. Seby, M. Point-Gautier, E. Giffaut, G. Borge, O. F. X. Donard, *Chem. Geol.* **2001**, *171*, 173.
[18] H. Hiura, T. W. Ebbesen, J. Fujita, K. Tanigaki, T. Takada, *Nature* **1994**, *367*, 148.
[19] A. Stabel, K. Eichhorst-Gerner, J. P. Rabe, A. R. Gonzalez-Elipe, *Langmuir* **1998**, *14*, 7324.
[20] H. Chang, A. J. Bard, *J. Am. Chem. Soc.* **1991**, *113*, 5588.
[21] J. V. Zoval, J. Lee, S. Gorer, R. M. Penner, *J. Phys. Chem.* **1998**, *102*, 1166.
[22] J. V. Zoval, P. Biernacki, R. M. Penner, *Anal. Chem.* **1996**, *68*, 1585.
[23] R. L. McCreery, in *Electroanalytical Chemistry*, Vol. 17 (Ed: R. L. McCreery), Marcel Dekker, New York **1991**, pp. 221–374.
[24] T. W. Ebbesen, M. E. Bisher, M. M. J. Treacy, J. L. Shreeve-Keyer, R. C. Haushalter, *Adv. Mater.* **1996**, *8*, 155.
[25] Y. Xia, Y. Ma, Y. Xing, Y. Mu, C. Tan, L. Mei, *Phys. Rev. B* **2000**, *61*, 11 088.
[26] H. Stahl, J. Appenzeller, R. Martel, P. Avouris, B. Lengeler, *Phys. Rev. Lett.* **2000**, *85*, 5186.
[27] H. R. Shea, R. Martel, P. Avouris, *Phys. Rev. Lett.* **2000**, *84*, 4441.
[28] W. Liang, M. Bockrath, D. Bozovic, J. H. Hafner, M. Tinkham, H. Park, *Nature* **2001**, *411*, 665.